Aeroelastic eigenvalue analysis of a variable speed rotor blade with an applied compressive load

Robert P. Dibble*, Vaclav Ondra†, Benjamin K. S. Woods‡ and Brano Titurus§
Department of Engineering, University of Bristol, Bristol, BS8 1TR, United Kingdom

Variable speed rotors are one possible way to meet the industry's increasing demands on noise emissions, flight envelopes and power requirements. The use of this technology is largely prohibited due to the presence of dynamic interactions at various rotor speeds that would lead to excessive vibratory loads. One concept being considered to overcome this is modal tuning by means of an applied compressive load. Herein, the impact of the combined effects of compressive loading, aerodynamic loading in hover and reduced rotor speeds on rotor blade's aeroelastic properties are investigated. A structurally nonlinear blade model directly coupled with an unsteady aerodynamic blade element model is formulated and verified. The model is used to show that moderate static deformations due to aerodynamic loads can introduce stiffening as well as softening effects. Compressive loading is then applied and it is shown that even at large compressive loads the blade's internal tension remains dominated by centrifugal loading. Finally, a study of the change in natural frequencies and damping ratios at various rotor speeds and compressive loadings is performed. It shows that natural frequencies and damping ratios are both affected by changing rotor speed and compressive load and that the sensitivity to the compressive load is greatest at lower rotor speeds.

Nomenclature

A	=	cross-sectional area, m^2
b	=	number of blades
c	=	aerofoil chord length, m
$C(k)$	=	Wagner function
$C_{l\alpha}$	=	lift coefficient gradient, rad^{-1}
C_{d0}	=	profile drag coefficient
D	=	profile drag force, N
e	=	distance between mass and elastic axis, m
e_A	=	distance between area centroid and elastic axis, m
E	=	Young's modulus of elasticity, Nm^{-2}
$F_{x'}, F_y, F_z$	=	internal shear forces in the x', y, z direction respectively, N
G	=	shear modulus of elasticity, Nm^{-2}
$I_{y'}, I_{z'}$	=	bending moments of inertia about major and minor neutral axes respectively, m^4
J	=	torsional stiffness constant, m^4
k	=	reduced frequency
k_A	=	polar radius of gyration of the cross-sectional area about the elastic axis, m
k_m	=	polar radius of gyration of the cross-sectional mass about the elastic axis, m
k_{m1}, k_{m2}	=	mass radii of gyration about the major axis and a perpendicular axis that intersects the elastic axis, m
L_{NC}, L_C	=	non-circulatory and circulatory aerodynamic force, Nm^{-1}
L_u, L_v, L_w	=	aerodynamic forces in the x,y,z axes, Nm^{-1}
m	=	mass distribution, kgm^{-1}
M_{aNC}, M_{aC}	=	non-circulatory and circulatory aerodynamic moment, N
$M_{x'}, M_{y'}, M_{z'}$	=	internal moments about the x', y', z' axes respectively, Nm

*PhD student, robert.dibble@bristol.ac.uk
†Research Associate, vaclav.ondra@bristol.ac.uk
‡Lecturer in Aerosopace Structures, ben.k.s.woods@bristol.ac.uk
§Senior Lecturer in Aerospace Dynamics, brano.titurus@bristol.ac.uk

M_ϕ	=	aerodynamic moment about the elastic axis, N
P	=	applied compressive load, N
P_{max}	=	maximum applied compressive load, N
P_x, P_y, P_z	=	forces in the x, y, z axes due to the compressive load, N
$P_{x'}, P_{y'}, P_{z'}$	=	forces in the x', y', z' axes due to the compressive load, N
R	=	radius of blade, m
R_0	=	root cutout of blade, m
s	=	complex number representing frequency, $rads^{-1}$
t	=	time, s
T	=	internal tension in the blade, N
T_{coord}	=	coordinate transfer matrix
u, v, w	=	lateral deformation in the x, y, z directions respectively, m
U, V, W, Φ	=	oscillatory shape component of u, v, w, ϕ respectively
U_0, V_0, W_0, Φ_0	=	static deformation component of u, v, w, ϕ respectively
v_{in}	=	inflow velocity, ms^{-1}
x, y, z	=	orthogonal coordinate system. x axis is the undeformed elastic axis. z axis is the axis of rotation, m
x', y', z'	=	local, deformed x, y, z axes. x axis is the deformed elastic axis.
α	=	effective angle of attack of the airflow to the plane of rotation, rad
β_{pc}	=	precone angle of the blade to the plane of rotation, rad
γ	=	combined response of blade, m
δ	=	linear twist as defined by $\theta\|_{x=R} - \theta\|_{x=R_0}$, rad
ϵ	=	scaling term to compare torsional deformation to transversal deformations, m
θ	=	blade pitch angle, prior to deformation, rad
λ	=	natural frequency, $rads^{-1}$
ρ	=	air density, kgm^{-3}
ρ_0	=	nominal air density, kgm^{-3}
ϕ	=	angle of torsional deformation about the elastic axis, rad
$\omega_\phi, \omega_v, \omega_w$	=	fundamental torsion, lead-lag, and flap frequencies, non-dimensionalised by Ω, as defined in [1]
Ω	=	rotor speed, $rads^{-1}$
Ω_0	=	nominal rotor speed, $rads^{-1}$
$\dot{[\ ]}$	=	derivative with respect to t
$[\ ]'$	=	derivative with respect to x

I. Introduction

The rotary wing sector strives towards developing aircraft with increased performance capability and reduced emissions. One concept to achieve this is variable speed rotors; which have been shown to require up to 70% less power [2], expand flight envelopes [3], reduce noise emissions [3, 4] and reduce fatigue (reducing operating costs and allowing for relaxed maintenance schedules [5]). This concept is utilised in the Boeing A160T Hummingbird [6] which holds the endurance record for new and experimental technologies at over eighteen hours [7], partly due to its ability to reduce its rotor speed by up to 40% [8].

Whilst variable speed rotors can achieve the desired performance improvements, they encounter significant dynamics complications which need to be overcome [3, 9]. If a rotor operates at a rotor speed with insufficient separation between natural and excitation frequencies, resonance will occur, which leads to increased vibratory loads that negatively affect the blade's structural performance and passenger comfort. Both natural and excitation frequencies are dependent on rotor speed; therefore, sufficient separation over a range of rotor speeds is difficult to achieve using solely the design of the blade's mass and stiffness distributions. Hence, rotorcraft are traditionally designed to operate at a single rotor speed with sufficient separation between all natural and excitation frequencies. If the benefits of variable speed rotors are to be fully utilised a method to avoid these resonances or minimise their consequences must be developed.

Existing active methods for vibration control, such as Active Control of Structural Response, Higher Harmonic Control and Individual Blade Control, may be adapted for use in overcoming the dynamics problems associated with variable speed rotors. However, active methods are often complex, heavy, and have significant power requirements. Embedded dampers on the other hand, are one passive method that have been explored to control transient loads in variable speed rotors [8]. However, passive systems are limited to a narrow bandwidth and are therefore unable to target multiple

resonances or remain effective when a change in rotor speed shifts the frequency of a resonance. Alternatively, resonance avoidance can be achieved in variable speed rotors by designing for stiff blades such that the blade's natural frequencies are sufficiently high to avoid interactions with the excitation frequencies with the most energy. However, this increase in stiffness can lead to a 34% increase in blade mass when compared to a conventional blade [2].

Centrifugal forces within a rotating rotor blade create restoring forces when the blade is perturbed from equilibrium. These restoring forces increase the effective stiffness of a rotor blade and the phenomenon is therefore known as *centrifugal stiffening* [10]. The concept investigated within uses an applied compressive load, which opposes the centrifugal forces, to induce a softening effect in the rotor blade and reduce its natural frequencies.

Modal tuning using structural loading has been investigated for application in transmission shafts [11] and helicopter fuselages [12]. In previous research by the authors [13, 14], the concept of using compressive loading for the modal tuning of rotor blades has been investigated in vacuo. Additionally, the effects of compressive axial loading on a rotor blade's static aeroelastic shape have been investigated [15]. The research presented herein aims to assess the impact of the combined effects of compressive loading, aerodynamic loading in hover and reduced rotor speeds on the rotor blade's natural frequencies and damping ratios. Whilst maintaining its focus on modal tuning using an applied compressive load, the present work is conceptually similar to research on aeroelastic stability of hingeless rotor blades presented in [1, 16].

The paper is organised as follows: in Section II the components of the model and the solution procedure are described. In Section III, the model is verified against available results. In Section IV, the model is used in a case study to assess the impact of compressive loading and a variable rotor speed on a rotor blade's dynamics on hover.

II. Mathematical model of a rotating blade subjected to compressive load

Previous research by the authors used linear models with no aerodynamic forcing [13, 14]. However, practical operational conditions require the influence of aerodynamic loading to be included. Therefore, an aeroelastic model for the modal properties of a hovering rotor blade with an applied compressive loading is developed.

The model presented within represents the concept depicted in Fig. 1. It is formulated as a Boundary Value Problem (BVP) in the rotating frame of reference and solved numerically using a collocation method.

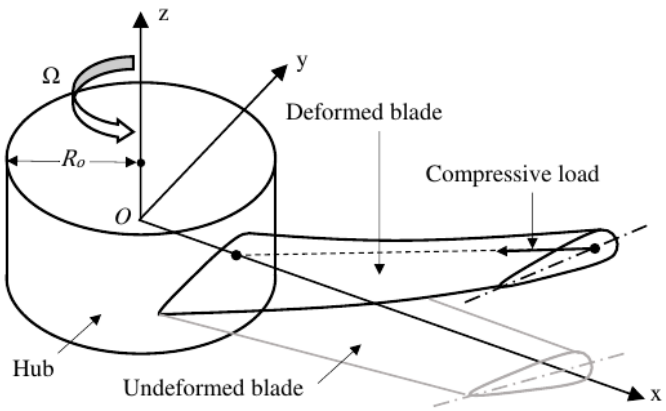

Fig. 1 Schematic of compressively loaded blade concept.

A. Boundary value problem formulation

This section introduces the BVP to be solved. Firstly, the field equations are described as a combination of the structural equations of motion coupled with the aerodynamic loads. Secondly, the boundary conditions are defined as a blade fixed at the root augmented by the compressive load. Lastly, the linearisation process for the dynamic analysis is explained.

1. Structural equations of motion

The structural equations of motion used were derived by Hodges and Dowell [17] and represent the coupled in-plane, out-of-plane and torsional motions of a rotating pretwisted beam with non-coincident mass and elastic axes. These

equations are ideally suited to model rotor blades as they are often pretwisted with offsets between their mass and elastic axes as well as having a high aspect ratio which makes it appropriate for them to be modelled as beams. There is no requirement to modify the equations to account for the compressive load. This load is applied at the tip and is therefore introduced to the model via the boundary conditions. As the structural equations of motion account for axial loads and deformations they are capable of capturing the propagation of the compressive load in their original form.
These equations are a set of four, nonlinear, non-homogenous, partial differential equations that have four states ϕ,u,v,w and are functions of one spatial domain, x and one temporal domain, t, as seen in Eqs. (1) to (5).

$$\begin{aligned}
&-\left[EAk_A{}^2(\theta+\phi)'\left(u'+\frac{v'^2}{2}+\frac{w'^2}{2}\right)\right]' - EAe_A\left(u'+\frac{v'^2}{2}+\frac{w'^2}{2}\right)(w''\cos\theta - v''\sin\theta) - (GJ\phi')' \\
&+(EI_{z'}-EI_{y'})\left[(w''^2-v''^2)\cos\theta\sin\theta + v''w''\cos 2\theta\right] + mk_m^2\ddot{\phi} + m\Omega^2\phi(k_{m2}{}^2-k_{m1}{}^2)\cos 2\theta \\
&+me[\Omega^2 x(w'\cos\theta - v'\sin\theta) - (\ddot{v}-\Omega^2 v)\sin\theta + \ddot{w}\cos\theta] = M_\phi - m\Omega^2(k_{m2}{}^2-k_{m1}{}^2)\cos\theta\sin\theta \\
&\qquad - me\Omega^2\beta_{pc}x\cos\theta
\end{aligned} \tag{1}$$

$$-T' - m(\Omega^2 x\underline{+2\Omega\dot{v}}) = L_u \tag{2}$$

$$\begin{aligned}
&-(Tv')' + \left[-EAe_A\left(u'+\frac{v'^2}{2}+\frac{w'^2}{2}\right)\cos(\theta+\phi) + [EI_{z'}\cos^2(\theta+\phi)+EI_{y'}\sin^2(\theta+\phi)]v''\right. \\
&\left.+(EI_{z'}-EI_{y'})\cos(\theta+\phi)\sin(\theta+\phi)w''\right]'' \underline{+2m\Omega\dot{u}} + m\ddot{v} - me\ddot{\phi}\sin\theta \\
&-2me\Omega(\underline{\dot{v}'\cos\theta+\dot{w}'\sin\theta}) - m\Omega^2[v+e\cos(\theta+\phi)]\underline{-2m\Omega\beta_{pc}\dot{w}'} \\
&\qquad -(me[\Omega^2 x\cos(\theta+\phi)\underline{+2\Omega\dot{v}\cos\theta}])' = L_v
\end{aligned} \tag{3}$$

$$\begin{aligned}
&-(Tw')' + \left[-EAe_A\left(u'+\frac{v'^2}{2}+\frac{w'^2}{2}\right)\sin(\theta+\phi) + (EI_{z'}-EI_{y'})\cos(\theta+\phi)\sin(\theta+\phi)v''\right. \\
&\left.+[EI_{z'}\sin^2(\theta+\phi)+EI_{y'}\cos^2(\theta+\phi)]w''\right]'' + m\ddot{w} + me\ddot{\phi}\cos\theta\underline{+2m\Omega\beta_{pc}\dot{v}} \\
&\qquad -(me[\Omega^2 x\sin(\theta+\phi)\underline{+2\Omega\dot{v}\sin\theta}])' = L_w - m\Omega^2\beta_{pc}x
\end{aligned} \tag{4}$$

where

$$T = EA\left(u'+\frac{v'^2}{2}+\frac{w'^2}{2}+k_A{}^2\theta'\phi' - e_A[v''\cos(\theta+\phi)+w''\sin(\theta+\phi)]\right) \tag{5}$$

In the original derivation, L_u, L_v, L_w, M_ϕ are generalised non-conservative forces and moments but for the purpose of this model they are to be used to incorporate the aerodynamic loading in to the field equations. Additionally, these equations contain terms proportional to the axial, in-plane, out-of-plane and torsional velocity - see underlined terms in Eqs. (1) to (5) - which are responsible for complex phase relationships between solved responses.

2. Aerodynamic loading

The aerodynamic loading applied to the blade is calculated as a set of distributed forces in- and out-of- the plane of rotation and a distributed torsional moment about the elastic axis of the blade. A two-dimensional unsteady blade element model, based on Greenberg's extension of Theodorsen's theory [18], is used to calculate these loads. Greenberg's approach calculates unsteady circulatory and non-circulatory forces and moments for an oscillating aerofoil. This aerodynamic model was aimed specifically for studies of forced dynamic responses of helicopter blades, making these equations ideally suited for this model. The aerodynamic loads are specified in Eq. (6) as follows.

$$
\begin{aligned}
L_u &= 0 \\
L_v &= -L_{NC}\sin(\theta+\phi) - L_C\sin(\alpha) - D\cos(\alpha) \\
L_w &= L_{NC}\cos(\theta+\phi) + L_C\cos(\alpha) - D\sin(\alpha) \\
M_\phi &= M_{aNC} + M_{aC}
\end{aligned}
\tag{6}
$$

where

$$
L_{NC} = \frac{1}{2}C_{l\alpha}\rho\frac{c^2}{4}\Big(- \ddot{w} + (\Omega x + \dot{v})\dot{\phi} + \ddot{v}(\theta+\phi) + \frac{c}{4}\ddot{\phi}\Big)
$$

$$
\begin{aligned}
L_C = C_{l\alpha}\rho(\Omega x + \dot{v})\frac{c}{2}\Big(&\Omega x(\theta+\Phi_0) + \dot{v}(\theta+\Phi_0)C(k) \\
&+ \big(\frac{c}{2}\dot{\phi} + \Omega x(\phi-\Phi_0)\big)C(k) - \dot{w}C(k)\underline{-v_{in}} + \dot{v}(\phi-\Phi_0)C(2k)\Big)
\end{aligned}
$$

$$
M_{aNC} = -\frac{1}{2}C_{l\alpha}\rho\frac{c^2}{4}\Big(- (\Omega x + \dot{v})^2(\theta+\phi) + \frac{c}{4}\ddot{v}(\theta+\phi) - (\Omega x + \dot{v})(-\dot{w}\underline{-v_{in}}) + \frac{c^2}{4}\frac{3}{8}\ddot{\phi} - \frac{c}{4}\ddot{w}\Big) \tag{7}
$$

$$
M_{aC} = -\frac{1}{2}C_{l\alpha}\rho(\Omega x + \dot{v})\frac{c^2}{4}\Big(- \dot{w}\underline{-v_{in}} + (\Omega x + \dot{v})(\theta+\phi) + \frac{c}{2}\dot{\phi}\Big)
$$

$$
D = \frac{1}{2}\rho\Big((v_{in}+\dot{w})^2 + (\Omega x + \dot{v})^2\Big)cC_{d0}
$$

$$
v_{in} = sign\Big((\theta+\Phi_0)|_{x=0.75R}\Big)\Omega\frac{bc}{8}\left(\sqrt{1 + \frac{12R}{bc}\Big|(\theta+\Phi_0)|_{x=0.75R}\Big|} - 1\right) \tag{8}
$$

$$
\begin{aligned}
\sin(\alpha) &= \frac{(v_{in}+\dot{w})}{\sqrt{(v_{in}+\dot{w})^2 + (\Omega x + \dot{v})^2}} \\
\cos(\alpha) &= \frac{(\Omega x + \dot{v})}{\sqrt{(v_{in}+\dot{w})^2 + (\Omega x + \dot{v})^2}}
\end{aligned}
\tag{9}
$$

and $C(k)$ is evaluated using Jones's approximation [19].

$$
\begin{aligned}
C(k) &\approx 1 - \frac{0.165}{1-(0.0455/k)i} - \frac{0.335}{(1-(0.3/k)i} \\
k &= \frac{Im(s)c}{2\Omega R}
\end{aligned}
\tag{10}
$$

L_{NC} is calculated as the integral of the pressure perpendicular to the chordline of the aerofoil, which is inclined to the plane of rotation at an angle, $\theta + \phi$. Therefore, this force needs to be decomposed in to components in the undeformed coordinate axes. Similarly, L_C is perpendicular to the local freestream flow, which is inclined to the plane of rotation at an angle, α and this force also needs to be decomposed in to components in the undeformed coordinate axes. These decompositions are performed by the trigonometric terms in Eq. (6).

The original equations derived by Greenberg [18] do not account for an inflow velocity. Therefore, the original equations are extended (similarly to [1]) to include an inflow velocity by substituting the terms $\dot{w}C(k)$ and $\dot{w}$ with the terms $\dot{w}C(k) + v_{in}$ and $\dot{w} + v_{in}$, respectively, see underlined terms in Eq. (7). The terms L_{NC},L_C,M_{aNC},M_{aC} are derived for an inviscid flow, therefore an additional force, D, for the profile drag is included in Eq. (6).
Defining the aerodynamic loading in this form allows Eq. (6) to be substituted directly in to Eqs. (1) to (5) forming a single set of aeroelastically coupled field equations. The presence of velocity terms and the complex value of the Wagner function further ensures that the dynamic response of the system will be complex.

3. Boundary conditions

Fixed boundary conditions are enforced to represent a bearingless hub as can be found in various modern helicopters. These boundary conditions are based on the those derived by Hodges and Dowell [17]. These conditions are then augmented by the forces associated with the compressive load to ensure equilibrium of the forces and moments at the tip of the blade. These conditions are implemented by constraining the displacements and slopes for the root, Eq. (11) evaluated at $x = R_0$

$$u = v = w = \phi = v' = w' = 0 \tag{11}$$

and loads at the tip of the blade, Eq. (12) evaluated at $x = R$.

$$\begin{aligned} F_{x'} &= -P_{x'} \\ F_y &= -P_y \\ F_z &= -P_z \\ M_{x'} = M_{y'} &= M_{z'} = 0 \end{aligned} \tag{12}$$

The following definitions of the sectional loads are adopted directly from [17]

$$M_{x'} = GJ\phi' + EAk_A{}^2(\theta + \phi)'\left(u' + \frac{v'^2}{2} + \frac{w'^2}{2}\right)$$

$$M_{y'} = EI_{y'}\left[v'' \sin(\theta + \phi) - w'' \cos(\theta + \phi)\right] \tag{13}$$

$$M_{z'} = -EAe_A\left(u' + \frac{v'^2}{2} + \frac{w'^2}{2}\right) + EI_{z'}\left[v'' \cos(\theta + \phi) + w'' \sin(\theta + \phi)\right]$$

$$F_{x'} = EA\left(u' + \frac{v'^2}{2} + \frac{w'^2}{2} + k_A{}^2\theta'\phi' - e_A\left[v'' \cos(\theta + \phi) + w'' \sin(\theta + \phi)\right]\right)$$

$$F_y = -M'_{y'} \sin(\theta + \phi) - M'_{z'} \cos(\theta + \phi) + F_{x'}v' - q_z \tag{14}$$

$$F_z = M'_{y'} \cos(\theta + \phi) - M'_{z'} \sin(\theta + \phi) + F_{x'}w' + q_y$$

where

$$
\begin{aligned}
q_x = m\Big(e\big[(\ddot{v} - \Omega^2 v)\sin(\theta+\phi) - \ddot{w}\cos(\theta+\phi) + 2\Omega\dot{u}\sin\theta\big] - {k_m}^2\ddot{\phi} \\
- \Omega^2({k_{m2}}^2 - {k_{m1}}^2)\cos(\theta+\phi)\sin(\theta+\phi) \\
- 2\Omega\big[({k_{m2}}^2 - {k_{m1}}^2)\dot{v}'\sin\theta\cos\theta + \dot{w}'({k_{m2}}^2\sin^2\theta + {k_{m1}}^2\cos^2\theta)\big]\Big)
\end{aligned}
\tag{15}
$$

$$
q_y = me(\Omega^2 x\sin(\theta+\phi) + 2\Omega\dot{v}\sin\theta)
$$

$$
q_z = -me(\Omega^2 x\cos(\theta+\phi) + 2\Omega\dot{v}\cos\theta) - \beta_{pc}q_x
$$

The applied compressive loads are calculated in the undeformed coordinate axes. However, for consistency with the axial force boundary condition in Eq. (12), they need to be transformed in to the local, deformed coordinate axes that are tangential to the deformed elastic axis. The transformation is performed using the transformation matrix available in [17] as follows

$$
\begin{bmatrix} P_{x'} \\ P_{y'} \\ P_{z'} \end{bmatrix} = \begin{bmatrix} 1 - \frac{v'^2}{2} - \frac{w'^2}{2} & -v'\cos(\theta+\phi) - w'\sin(\theta+\phi) & v'\sin(\theta+\phi) - w'\cos(\theta+\phi) \\ v' & \left(1 - \frac{v'^2}{2}\right)\cos(\theta+\phi+v'w') & -\left(1 - \frac{v'^2}{2}\right)\sin(\theta+\phi+v'w') \\ w' & \left(1 - \frac{w'^2}{2}\right)\sin(\theta+\phi+v'w') & \left(1 - \frac{w'^2}{2}\right)\cos(\theta+\phi+v'w') \end{bmatrix}^{-1} \begin{bmatrix} P_x \\ P_y \\ P_z \end{bmatrix} \tag{16}
$$

4. Compressive load

The applied compressive load is modelled solely as a tip force, as this allows the effects of the force to be isolated from any secondary effects associated with a load application system [14].

The force is located at the tip, directed towards the root as these are likely attachment points of any load application system. The force is decomposed into constituent forces along the undeformed x, y, z axes, similarly to [20], to be applied in the shear force boundary conditions defined in Section II.A.3. The decomposition of the forces can be seen in Fig. 2 and Eq. (17).

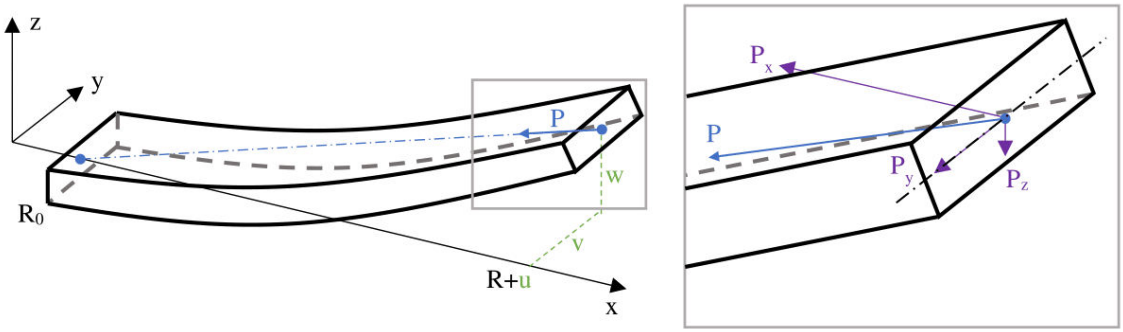

Fig. 2 Schematic of compressive force directed towards root of blade.

$$
\begin{aligned}
P_x &= P\frac{R - R_0 + u}{\sqrt{(R - R_0 + u)^2 + v^2 + w^2}} \\
P_y &= P\frac{v}{\sqrt{(R - R_0 + u)^2 + v^2 + w^2}} \\
P_z &= P\frac{w}{\sqrt{(R - R_0 + u)^2 + v^2 + w^2}}
\end{aligned}
\tag{17}
$$

The decomposition of this load creates transversal forces that oppose the tip deformation. It can be shown that these restoring forces result in a buckling load four times greater than the prediction by the traditional Euler buckling method [20].

5. Linearisation procedure

To solve the nonlinear equations described in Sections II.A.1 to II.A.4, it is assumed that the solution takes the form of a static time-invariant deformation combined with a small harmonic oscillation. Thus the assumed solution is written as follows Eq. (18)

$$\begin{aligned} u(x,t) &= U_0(x) + U(x)e^{st} \\ v(x,t) &= V_0(x) + V(x)e^{st} \\ w(x,t) &= W_0(x) + W(x)e^{st} \\ \phi(x,t) &= \Phi_0(x) + \Phi(x)e^{st} \end{aligned} \tag{18}$$

In this research, the harmonic oscillation terms take the form e^{st}, where s represents frequency, denoted in a complex form to correspond with the form used for the natural frequency. The imaginary component of s represents the damped frequency and the real component relates to damping.

This form allows the problem to be separated in to two distinct BVPs; one for the static deformation of the blade and one for the small oscillations about that deformation. A linearisation of the field equations and boundary conditions described in Sections II.A.1 to II.A.4 is performed to provide the separate field equations and boundary conditions for each BVP.

Terms which are constant with respect to time are gathered to form a set of ordinary differential equations and boundary conditions which represent the static deformation of the blade. This BVP retains its nonlinear characteristic with respect to its states, U_0, V_0, W_0, Φ_0.

Terms which are linear with respect to the time dependant part of the assumed solution are gathered to form a set of partial differential equations that represent the small harmonic motion of the blade about the static deformation. The principle of separation of variables is employed to split the spatial and temporal components of the solution. The e^{st} terms are dropped, resulting in a BVP defined solely on the spatial domain. The coefficients of these linearised equations are functions of the static deformation. This is how the influence of the static deformation on the dynamics is captured. Remaining terms are the product of two or more oscillatory terms. As these oscillatory terms are small with respect to the static terms, their product is considered negligible and they are therefore omitted.

Eqs. (9) and (17) contain the states U, V, W, Φ in the denominator of a fraction. It is not possible to use these terms in the previously described linearisation process directly. Therefore, the Taylor expansion of these equations about the static deformation is used. The expansion includes terms which are constant and linearly proportional to the time dependant part of the assumed solution; higher order terms are neglected to stay consistent with the linearisation process.

B. Numerical solution procedure

1. BVP solver

The dynamics BVP can be used to provide two different types of solution. One solution, herein referred to as a *harmonic* solution, uses a prescribed value of s to obtain the response shape of the blade when excited at a frequency ω where $s = i\omega$.

The second solution type, herein referred to as an *eigenvalue* solution includes s as an unknown parameter. This solution type represents the natural frequency of the blade. Additionally, for an *eigenvalue* solution, the combined response at the tip, Eq. (19), is used to provide the normalisation condition.

$$\gamma^2 = \left| u^2 + v^2 + w^2 + (\epsilon\phi)^2 \right| \tag{19}$$

A solver in MatLab, *bvp4c*, numerically solves the BVP using a collocation method [21]. The solver uses cubic polynomials between collocation points to define candidate solutions. Finite differences are used to implement a

three-stage Lobatto IIIa method which minimises residuals across the domain [22]. Mesh distribution and convergence criteria are determined based on the residuals of the candidate solution.
The solver requires that the field equations are provided as a system of first order ordinary differential equations with a corresponding set of boundary conditions. An initial estimate for the solution is required; the quality of this estimate dictates the computational time and the ability of the solver to converge to the correct solution. Provided that a suitable initial estimate is provided, the solver is very versatile and robust. This allows it to be used to solve both the nonlinear static deformation BVP and the complex dynamics BVP.

2. Sequential parametric sweep procedure

To calculate the natural frequencies over a range of operating and loading conditions a two-part iterative sweep procedure is used. In the first part, the natural frequencies of the desired modes are calculated for a single value of the compressive load and rotor speed. Once the natural frequencies of the desired modes have been obtained, the second part incrementally sweeps through the range of compressive load and rotor speed values and calculates the natural frequencies.
The first part, to calculate the natural frequencies at a single value of compressive load and rotor speed, uses a combination of *harmonic* and *eigenvalue* analyses. Firstly, a static analysis is performed to calculate the static deformation of the blade about which the small dynamic oscillations occur. Subsequently, a series of *harmonic* analyses are performed to calculate the response shape at the prescribed frequencies, starting at $s \approx 0 + 0i$, and then increasing the imaginary component representing frequency, akin to a stepped sine sweep. These response shapes are then used to identify the presence of a mode. If a mode is detected, *eigenvalue* analysis is performed to calculate the natural frequency more precisely. For the first *harmonic* analysis, the initial estimate provided to the solver is an analytically calculated fundamental bending modeshape of an uncoupled, non-rotating beam as this is a similar shape to the first mode to be identified. Subsequent *harmonic* analyses use the solution from the previous iteration as the initial estimate. For the *eigenvalue* analyses, the solution of the nearest resonant *harmonic* analysis is used as the initial estimate. This process is repeated until the desired number of modes have been obtained or the desired range of frequencies has been evaluated. See Fig. 3 for a pseudo-code description of this process.

```
Omega = initial rotor speed
P = initial compressive load
s = ~ 0
initial shape = analytical solution
while not all modes found
    forced response = harmonic analysis (initial shape)
    if response indicates mode
        eigenvalue = eigenvalue analysis (forced response)
    end
    s = s + Δs
    initial shape = forced response
end
```

Fig. 3 Process of natural frequency and mode shape calculation for initial rotor speed and compressive load

Once the natural frequencies are calculated for a single value of rotor speed and compressive load in part one, the natural frequencies for all the combinations of the predefined rotor speeds and compressive loadings are calculated. Firstly, a sweep of rotor speeds is performed while the compressive load remains constant. The rotor speed is incrementally increased, a static analysis is used to calculate the static deformation of the blade, and then an *eigenvalue* analysis is performed to calculate natural frequency for each mode in turn. The initial estimate provided for each *eigenvalue* analysis is the solution for that mode from the previous rotor speed. Once one rotor speed sweep is completed, the compressive load is incrementally increased and the previously described sweep of rotor speed values is repeated. This procedure results in natural frequencies for each desired combination of rotor speed and compressive loading.

III. Model verification

Previous research [13] has demonstrated the capability of this modelling methodology to capture the required structural behaviour, including the applied compressive load.
To ensure that aeroelastic elements of the model described in Section II have been correctly implemented, the present model is compared with [1]. The blade properties used for this comparison study correspond to those used in the reference work and are presented in Table 1.

Table 1 Blade properties and operating conditions for verification case

Property	Value	Property	Value	Property	Value
$(k_A/k_m)^2$	1.5	b	4	ω_ϕ	5
k_m/R	0.025	$C(k)$	1	ω_v	0.7
k_{m1}/k_{m2}	0	$C_{l\alpha}$	2π	ω_w	1.15
$3\rho C_{l\alpha} cR/m$	5	C_{d0}	0.01	e	0
$\frac{c}{R}$	$\frac{\pi}{40}$	δ	0	e_A	0

Torsional, in-plane and out-of-plane static deformations at the blade tip as well as the natural frequencies for the modes presented in [1] - first torsional (T_1), out-of-plane (O_1) and in-plane (I_1) modes - are calculated for a range of blade pitch angles. These results are compared with those obtained in [1] in Fig. 4.

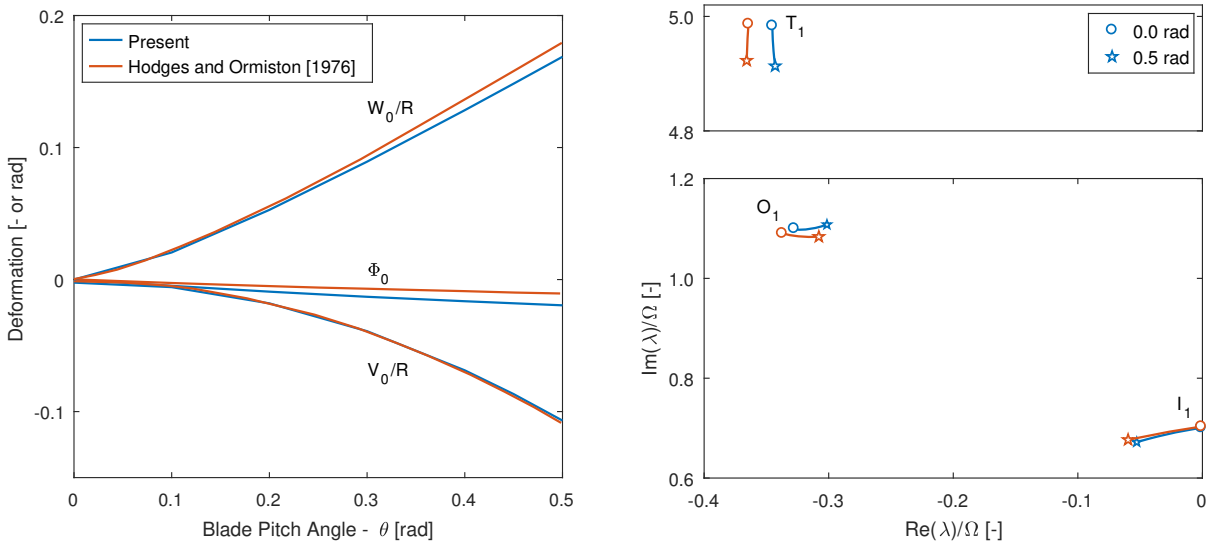

(a) Static deformation

(b) Natural frequencies

Fig. 4 Comparison of results from the present model with those from [1].

It can be seen that the static deformations in Fig. 4(a) and the natural frequencies in Fig. 4(b) calculated in the present model are in agreement with the published results.
The differences observed may be attributed to a few separate discrepancies between the two models. Firstly, in [1], the solutions are obtained using a two-stage Galerkin method, initially using uncoupled, non-rotating modeshapes whereas the present model uses a collocation method which uses cubic polynomials to define candidate solutions. Secondly, trigonometric terms in the aerodynamic model were treated using a small angle assumptions in [1] whereas in the present model, a Taylor expansion is used. Additionally, due to the coupled nature of the model, errors will propogate between different deformation directions as well as from the static deformation to the natural frequencies. For instance, in the present work, there is a small overestimate of the negative torsional static deformation which will reduce the amount of lift. This reduction in lift may be a cause of the underestimation of the out-of-plane static deformation and

torsional damping.
Overall, the agreement is good which gives confidence that the model has been developed and implemented correctly.

IV. Rotor blade case study

The subsequent section uses the model in a case study to investigate the effects of aerodynamic and compressive loading on the natural frequencies of a variable speed rotor blade. Firstly, the effect of static deformation due to aerodynamic loading on the blade frequencies shall be considered. Secondly, the effect of compressive loading on the static deformation shall be investigated. Finally, a study of the influence of compressive loading on a rotor blade's natural frequencies and damping ratios at various rotor speeds is performed.
The rotor blade considered is a hingeless blade with properties and operating conditions similar to that of an MBB Bo 105 [23], as summarised in Table 2. The model described in Section II is used to calculate the frequencies of the first torsion (T_1), first two in-plane modes (I_1-I_2) and first three out-of-plane modes (O_1-O_3).
A lower limit of 60% of the nominal rotor speed is used in order to replicate the 40% reduction used by the A160T Hummingbird [8]. To ensure that a buckling instability is not approached by the compressive loading, a maximum load to be applied is introduced. The maximum load is set to be 75% of the critical buckling load, calculated at the lowest rotor speed to ensure a conservative limit. The critical buckling load is defined as the load at which the lowest natural frequency equals zero [20, 24].

Table 2 Blade properties and operating conditions for case study blade

Property	Value	Property	Value	Property	Value
$E\ [N.m^{-2}]$	69	$A\ [m^4]$	$2.80x10^{-3}$	$c\ [m]$	0.275
$G\ [N.m^{-2}]$	26.5	$\theta\|_{x=R_0}\ [rad]$	0.436	$\rho_0\ [kg.m^{-3}]$	1.225
$R\ [m]$	4.91	$\delta\ [rad]$	−0.140	C_{d0}	0.01
$R_0\ [m]$	1.03	$e\ [m]$	0	$C_{l\alpha}\ [rad^{-1}]$	2π
$I_{y'}\ [m^4]$	$9.92x10^{-8}$	$e_A\ [m]$	0	$P_{max}\ [N]$	$9.52x10^3$
$I_{z'}\ [m^4]$	$2.47x10^{-6}$	$m\ [kg.m^{-1}]$	7.55		
$J\ [m^4]$	$1.65x10^{-7}$	$\Omega_0\ [rad.s^{-1}]$	44.51		

A. Influence of state deformation on natural frequencies

In the subsequent section, the effect of the static deformation is isolated by removing the aerodynamic forcing from the dynamics BVP. To assess the influence of static deformation on natural frequencies, the air density in the static analyses is varied from zero to ρ_0 to alter the static deformation which will in turn impact the natural frequencies. The static deformations at the tip of the blade are shown in Fig. 5.

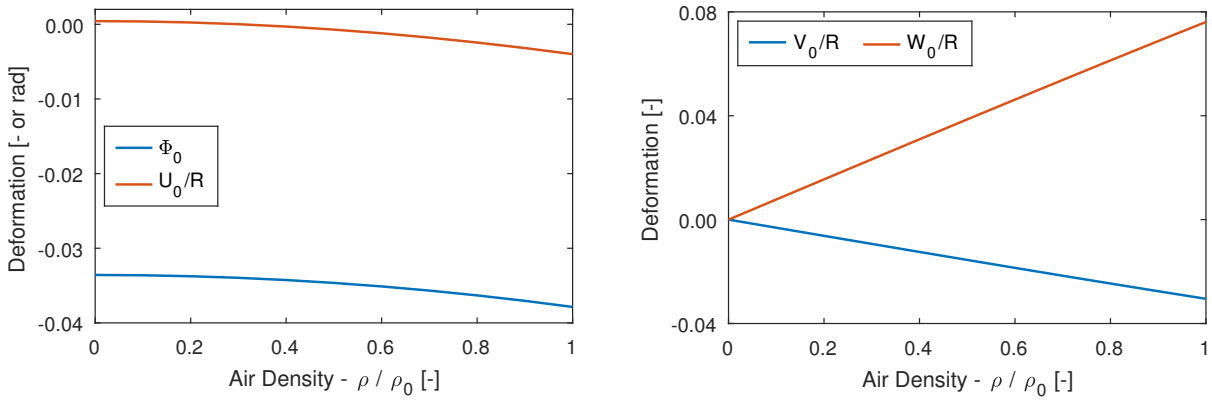

(a) Torsional and axial

(b) In-plane and out-of-plane

Fig. 5 Static deformation of the blade at its tip

It can be seen in Fig. 5(a) that in vacuo there is a negative torsional deformation which is due to the centrifugal loads opposing the positive blade pitch angle. The torsional deformation decreases as air density increases is not due to aerodynamic torque as this is zero due to the coincident aerodynamic centre and elastic axis and implied airfoil symmetry observed in [18]. Instead, the decrease in torsional deformation is thought to be due to the negative in-plane deformation coupled with the positive out-of-plane deformation which then results in a negative torsional deformation. This phenomenon is similar to that observed in rearward swept fixed-wing aircraft which use it to increase the static divergence speed.

In vacuo, there is a small positive axial extension due to the centrifugal loads stretching the blade axially. As the air density, and therefore aerodynamic loads, increase there is an increase in in-plane and out-of-plane deformation which leads to a geometric shortening of the blade. This effect is much greater than the extension due to centrifugal loads resulting in a net shortening of the blade.

It can be seen in Fig. 5(b) that in vacuo, there is no in-plane or out-of-plane deformation which is due to the lack of aerodynamic loads and off-axis inertial loads. As the air density increases, the in-plane and out-of-plane deformation also increases. It can be seen that these deformations are in excess of an order of magnitude larger than the axial deformation due to centrifugal loads.

As the static deformation increases, there may be an influence on the rotor blade's natural frequencies. Therefore, the change in the natural frequencies is shown in Fig. 6.

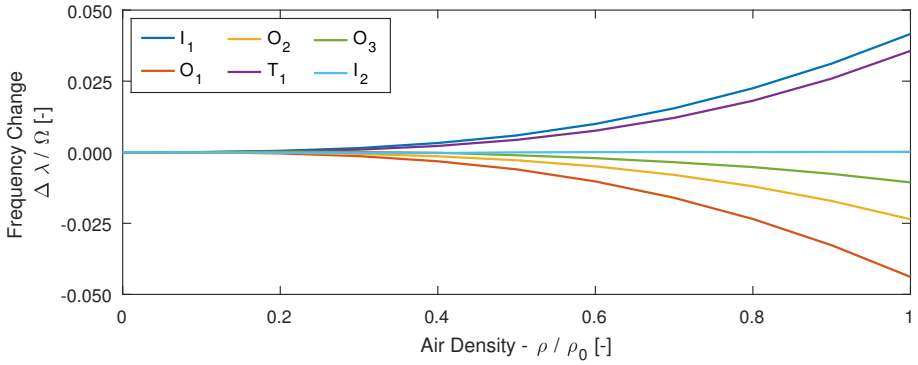

Fig. 6 Change in the natural frequencies with increasing static deformation

When avoiding resonance in rotor blades, the desired minimum separation between natural and excitation frequencies is approximately 10% of the rotor speed. Therefore, the magnitude of changes seen in Fig. 6 of up to $\sim$ 4% are considered significant. Consequently, the influence of the blade's deformed static shape should be considered when investigating resonance avoidance.

Additionally, it can be seen that the natural frequencies of the torsional and in-plane modes increase, whereas the

out-of-plane modes decrease. The trend of increasing natural frequencies with increasing static deformation has been observed in fixed-wing aircraft [25]. However, this trend was observed for all modes of interest. The decrease in the natural frequency of the out-of-plane modes may be attributable to the reduction in the induced centrifugal loads caused by the geometric shortening of the statically deformed blades, as observed in Fig. 5(a). Whilst all modes will be affected by the reduced centrifugal loads, the frequencies of the out-of-plane modes are the most influenced by this loading and will therefore be most strongly affected by a reduction in it.

B. Influence of compressive loading on static deformation

It has been shown that the static deformation due to aerodynamic loading has a considerable impact on the blade's dynamics, therefore the impact of compressive loading on the rotor blade's static deformation is investigated. The impact of compressive loading on the rotor blade dynamics with no aerodynamic forcing in the dynamics BVP shall not be covered as this has been investigated previously [13, 14]. This study is performed at the lowest rotor speed to reduce the effects of centrifugal loading and accentuate the impact of the compressive loading. The static deformation for no compressive load and with the maximum compressive load is shown in Fig. 7.

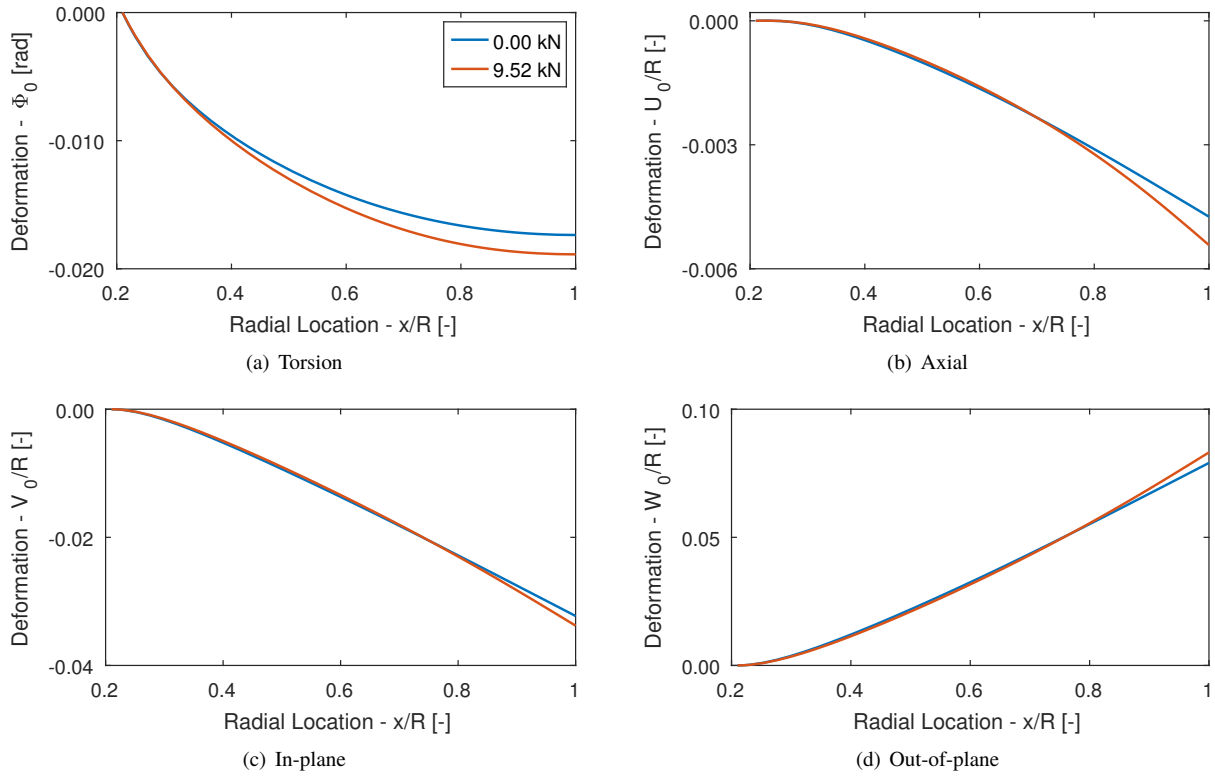

(a) Torsion (b) Axial

(c) In-plane (d) Out-of-plane

Fig. 7 Effect of the compressive load on static deformation

It can be seen in Fig. 7(a) that there is a negative torsional deformation, due to the inertial and aerodynamic loads described in Section IV.A. Additionally, it should be noted that the blade pitch angle at the tip is 0.296 rad, compared to the deformation of -0.017 rad, therefore the blade's geometry remains the dominant influence on the aerodynamic angle of attack. The softening effect induced by the compressive load reduces the effective stiffness of the blade, increasing the deformation due to inertial and aerodynamics loads. However it should be noted that the largest change in deformation is 0.00152 rad which will results in a negligible effect on the aerodynamic loads.
It can be seen in Fig. 7(b) that, as in Section IV.A, the deformations are small (<1% of the radius) and dominated by geometric shortening. The application of a compressive load increases the shortening of the blade which is due to the direct compression of the blade and the increased geometric shortening due to the increase in-plane and out-of-plane deformation.

Figs. 7(c) and 7(d) show that the in-plane and out-of-plane deformation remain the largest deformations. The out-of-plane deformation is the larger of the two due to the larger aerodynamic load and lower stiffness. Both of these deformations exhibit an increased deformation at the tip and a reduced deformation at the mid-span. Therefore, the compressive loading can be seen to increase the curvature of the blade which will result in greater stresses.
It should also be noted that despite the compressive load being 75% of the buckling load, the changes in deformation are small. This behaviour agrees with previous studies where the abruptness of the onset of buckling has been demonstrated [15].
Despite the small changes in the blade's static deformation due to compressive load, it has been shown that loads of this magnitude can induce significant change in the blade frequencies. Therefore, the tension distribution in the blade, as defined by Eq. (5), with no compressive load and with the maximum compressive load are shown in Fig. 8. For comparison, the analytical solution used in [13] is shown alongside.

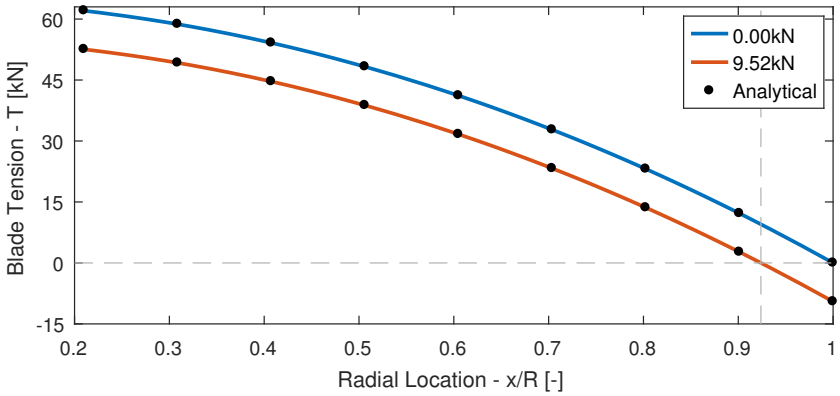

Fig. 8 Effect of compressive loading on internal blade tension.

It can be seen that when the blade has no applied compressive load, the tension distribution follows the parabolic shape of the analytical solution, used in [13], with a large root load and zero load at the tip. Despite the magnitude of these loads, the axial deformation observed in vacuo in Fig. 5(a) is small due to the large axial stiffness, EA, of the rotor blade.
When the rotor blade is loaded with the maximum compressive load, the internal tension in the blade remains dominated by the centrifugal forces; only a small portion of the blade is in compression ($T < 0$ when $x/R > 0.92$ as indicated in Fig. 8).
The reduction in tension due to the compressive load is approximately constant with a reduction of 9.503 kN at the root and 9.505 kN at the tip. Both of these loads are marginally less than the applied 9.52 kN compressive load because of the decomposition described in Section II.A.4. The approximately constant reduction in internal tension and the correlation with the analytical solution justifies its use in previous work [13, 14].

C. Compressive loading influence on dynamics of variable speed rotor blades

Previous research on the effects of compressive loading on the dynamics of variable speed rotor blades has focused solely on the dynamics of the rotor blade and excluded the effects of aerodynamics. In the subsequent section, the present aeroelastic model is used in full to investigate the effects of compressive loading on the natural frequencies and damping ratios of a variable speed rotor blade in hover.
Root locus plots are shown in Fig. 9 to illustrate how the natural frequencies and damping ratios change with rotor speed and compressive load as well as how these trends compare with those observed in previous work. These plots are calculated at 60% and 100% of the nominal rotor speeds with a compressive load between $0\,kN$ and $9.52\,kN$, as in Section IV.A.

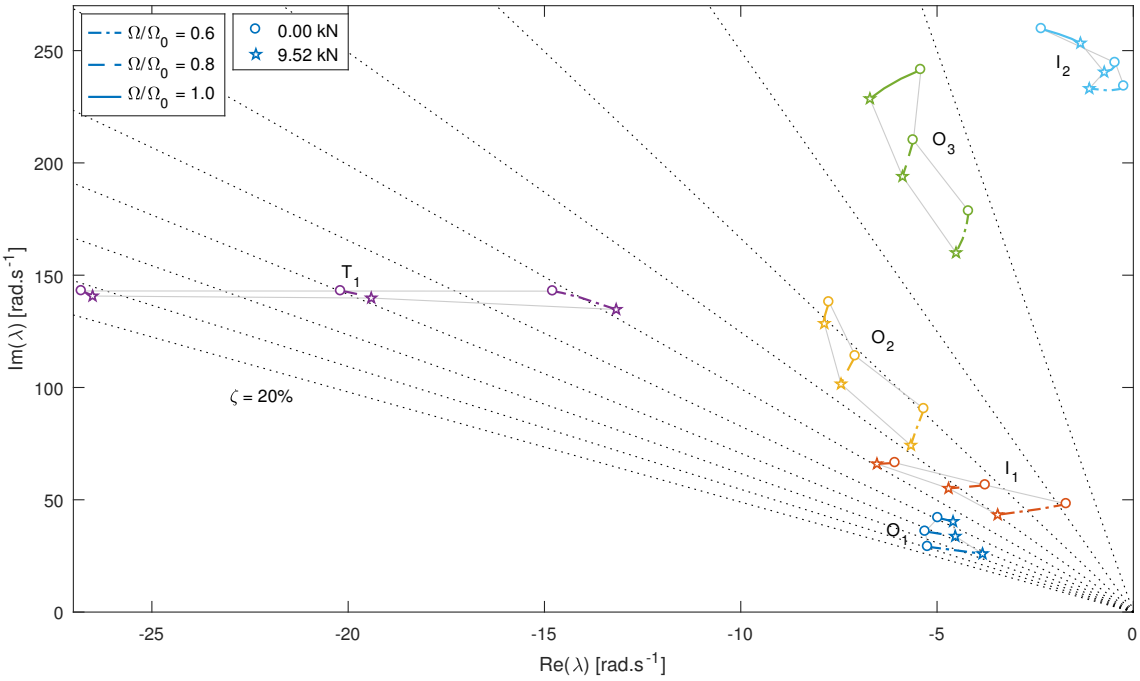

Fig. 9 Root locus plots for modes of interest as compressive load is increased. Radial lines denote constant damping ratio increments of 2%.

It can be seen that the natural frequencies exhibit the same trends as those observed in previous work. Firstly, all of the modes increase in frequency at the higher rotor speed due to the increase in centrifugal loads. Secondly, all of the natural frequencies are less sensitive to the compressive loading at the higher rotor speed, which is due to the increased dominance of the centrifugal forces. Therefore, if utilised in a modal tuning based resonance avoidance system with a fixed maximum load, there will be greater influence of the frequencies, and therefore greater control, available at lower rotor speeds.

The novel aspect of this research, compared to previous work, is the aeroelastic nature of the model which captures the aerodynamic damping present in each mode and how it changes under the influence of compressive loading.

It can be seen in Fig. 9 that the change in rotor speed, with no compressive loading, can significantly alter the damping ratios. The damping ratios of the torsional and in-plane modes can be seen to increase with increasing rotor speed (by approximately 8%, 5%, 1% for T_1, I_1, I_2, respectively) which is likely caused by the increase in magnitude of the aerodynamic forces due to the increased rotor speed. However, the damping ratios of the out-of-plane modes either remain approximately constant (O_2,O_3) or reduce (by approximately 6% for O_1).

The application of compressive load can also be seen to alter the damping ratios. For all modes, the magnitude of the change in damping ratios due to compressive loading at the lowest rotor speed is similar or greater than the change observed at the highest rotor speed which agrees with the previous discussion that there is more sensitivity to the compressive load at lower rotor speeds.

The first in-plane and second and third out-of-plane modes exhibit an increased damping ratio with compressive load for both rotor speeds. This trend may be utilised to reduce the amount of separation required in these modes due to an increase in their damping ratio.

As with the trend in damping ratio due to rotor speed, the first out-of-plane modes exhibits the opposite behaviour as its damping ratio reduces with compressive load for both rotor speeds. The tendency of the first out-of-plane mode to exhibit differing trends to the other modes is of particular interest and will require further validation and investigation to identify its cause.

Finally, it can be seen that first torsional and second in-plane mode exhibit a different trends of increasing or decreasing damping ratio with compressive load at the highest rotor speed than they do at the lower rotor speeds. This is likely to be due to the proximity of their natural frequencies to the second and third out-of-plane modes, respectively, which will result in coupling between these modes. As the compressive loading increases the frequency of the out-of-plane modes decreases and so does the coupling. This shows that coupling influences not only the natural frequency, but the damping

ratios too.

V. Conclusion

The research presented in this paper extends beyond previous work on compressive loading based modal tuning for variable speed rotors as it includes structural non-linearities and aerodynamic forcing. The results presented show that the static deformation due to aerodynamic loading significantly influences the natural frequencies of the first six modes of a rotor blade but that compressive loading has a small effect on the static deformation. Compressive loading and variable rotor speeds have been shown to significantly alter the natural frequencies and damping ratios of the first six modes of a rotor blade. It was shown that at lower rotor speeds, the modes are more sensitive to compressive loading which will result in greater modal tuning control being available. Additionally, it was shown that the compressive loading significantly alters the damping ratios of all modes; in general, they increase with compressive load. The damping ratio of the first out-of-plane mode exhibited counter-intuitive trends with respect to rotor speed and compressive load that opposed those of the other modes.

To summarise, modal tuning systems should be designed using a model that captures structural non-linearities and aerodynamic loading as these have been shown to be significant. Additionally, design studies should be performed using a more appropriate metric than frequency separation, such as vibratory loads, as this will allow the effects of damping ratios, and their changes due to compressive loading, to be captured. Future studies will further validate the model and investigate the causes of some of the behaviours presented here such as the influence of static deformation on natural frequencies and the impact of compressive load on damping ratios.

Acknowledgments

R. Dibble would like to thank The UK Vertical Lift Network and ESPRC for their support and funding. V. Ondra, B.Woods and B. Titurus would like to acknowledge the financial support of the European Community's Horizon 2020 Program provided through the project "Shape Adaptive Blades for Rotorcraft Efficiency (SABRE)", Grant Agreement 723491.

References

[1] Hodges, D. H., and Ormiston, R. A., "Stability of elastic bending and torsion of uniform cantilever rotor blades in hover with variable structural coupling," Tech. rep., 1976.

[2] Karem, A. E., *Optimum speed rotor*, 1999. U.S. Patent No. 6,007,298.

[3] Misté, G. A., and Benini, E., "Variable-Speed Rotor Helicopters: Performance Comparison Between Continuously Variable and Fixed-Ratio Transmissions," *Journal of Aircraft*, Vol. 53, No. 5, 2016, pp. 1189–1200.

[4] Allongue, M., Marze, H. J., and Potdevin, F., "The Quiet Helicopter 'from research to reality'," *55th Annual AHS Forum Proceedings*, 1999, pp. 87–103.

[5] du Bois, J. L., Lieven, N. A. J., and Adhikari, S., "A tensioned cable as an adaptive tuned vibration absorber for response suppression in rotorcraft," *25th International Conference on Noise and Vibration engineering, ISMA2012 in conjunction with the 4th International Conference on Uncertainty in Structural Dynamics, USD 2012*, Vol. 1, 2012, pp. 237–250.

[6] Putrich, G., "FARNBOROUGH: Cutaway & technical description: Defying convention - Boeing A160 Hummingbird," *Flightglobal*, 2010.

[7] *Record ID 15059*, Fédération Aéronautique Internationale, 2008. Http://archive.li/u8aZT.

[8] Han, D., Wang, J., Smith, E. C., and Lesieutre, G. A., "Transient Loads Control of a Variable Speed Rotor During Lagwise Resonance Crossing," *AIAA Journal*, Vol. 51, No. 1, 2013, pp. 20–29. doi:Doi10.2514/1.J050598.

[9] Han, D., and Smith, E. C., "Lagwise dynamic analysis of a variable speed rotor," *Aerospace Science and Technology*, Vol. 29, No. 1, 2013, pp. 277–286.

[10] Newman, S., *Foundations of helicopter flight*, Elsevier, 1994.

[11] Turkstra, T., and Semercigil, S., "Elimination of Resonance with a Switching Tensile Support," *Journal of Sound and Vibration*, Vol. 163, No. 2, 1993, pp. 359–362.

[12] du Bois, J. L., Lieven, N. A. J., and Adhikari, S., "Adaptive Passive Control of Dynamic Response Through Structural Loading," *48th AIAA/ASME/ASCE/AHS/ASC Structures, Structural Dynamics, and Materials Conference*, 2007, pp. 1–14.

[13] Dibble, R. P., and Titurus, B., "Helicopter rotor blade modal tuning using internal preloads," *International Seminar on Modal analysis*, Leuven, Belgium, 2016.

[14] Ondra, V., Dibble, R. P., and Titurus, B., "Towards an application of an active tendon in rotorcraft: A numerical and experimental study of coupled bending-torsion vibration of a beam-tendon system," *International Seminar on Modal analysis*, Leuven, Belgium, 2018.

[15] Dibble, R. P., Woods, B., and Titurus, B., "Static Aeroelastic Response of a Rotor Blade Under Internal Axial Loading," *European Rotorcraft Forum*, Milan, Italy, 2017.

[16] Amoozgar, M. R., Shahverdi, H., and Nobari, A. S., "Aeroelastic Stability of Hingeless Rotor Blades in Hover Using Fully Intrinsic Equations," *AIAA Journal*, Vol. 55, No. 7, 2017, pp. 2450–2460.

[17] Hodges, D. H., and Dowell, E. H., "Nonlinear equations of motion for the elastic bending and torsion of twisted nonuniform rotor blades," Tech. rep., NASA Technical Note D-7818, 1974.

[18] Greenberg, J. M., "Airfoil in sinusoidal motion in a pulsating stream," *NATIONAL ADVISORY COMMITTEE FOR AERONAUTICS TECHNICAL NOTE 1326*, , No. 1326, 1947.

[19] Jones, R. T., "Operational Treatment of the Nonuniform Lift Theory in Airplane Dynamics," Tech. rep., NACA Technical Note 667, Oct. 1938.

[20] Nudehi, S., Mukherjee, R., and Shaw, S. W., "Active Vibration Control of a Flexible Beam Using a Buckling-Type End Force," *Journal of Dynamic Systems, Measurement, and Control*, Vol. 128, No. 2, 2006, pp. 278–286.

[21] Shampine, L. F., Kierzenka, J., and Reichelt, M. W., "Solving boundary value problems for ordinary differential equations in MATLAB with bvp4c," Tech. rep., Tutorisl notes 75275, 2000.

[22] Kierzenka, J. A., and Shampine, L. F., "A BVP Solver Based on Residual Control and the MATLAB PSE," *ACM Transactions on Mathematical Software*, Vol. 27, No. 3, 2001, pp. 299–316.

[23] Staley, J. A., "Validation of Rotorcraft Flight Simulation Program through Correlation with Flight Data for Soft-in-Plane Hingeless Rotors," Tech. rep., AMRDL-TR-75-50, 1976.

[24] Virgin, L. N., *Vibration of Axially-Loaded Structures*, Cambridge University Press, 2007.

[25] Nguyen, N. T., Ting, E., and Lebofsky, S., "Aeroelasticity of Axially Loaded Aerodynamic Structures for Truss-Braced Wing Aircraft," *56th AIAA/ASCE/AHS/ASC Structures, Structural Dynamics, and Materials Conference*, 2015, p. 1840.